Soil Dynamics and Earthquake Engineering 88 (2016) 143–151

Contents lists available at ScienceDirect

Soil Dynamics and Earthquake Engineering

journal homepage: www.elsevier.com/locate/soildyn

Small-strain stiffness of sand subjected to stress anisotropy

Meghdad Payan, Arman Khoshghalb, Kostas Senetakis, Nasser Khalili *

School of Civil and Environmental Engineering, UNSW Australia, Sydney 2052, Australia

ARTICLE INFO

Article history:
Received 16 March 2016
Received in revised form
6 June 2016
Accepted 9 June 2016

Keywords:
Small-strain shear modulus
Anisotropic stress state
Bender elements

ABSTRACT

Stiffness of soils at small strains expressed through the small-strain shear modulus is critical for the evaluation of deformations of geo-structures subjected to a variety of stress states. While most of the previous studies of small-strain shear modulus of sands have focused on the isotropic stress state, there exist innumerable situations in geotechnical engineering in which the soil is under an anisotropic stress state. In this study, the influence of stress anisotropy on the small-strain shear modulus (G_{max}) of sands is evaluated using the results of a comprehensive set of bender element tests conducted on saturated sand samples under isotropic and anisotropic loading conditions. It is shown that the small-strain shear moduli of sands under anisotropic loading conditions are greater in magnitude than those subjected to isotropic stress states at a given mean effective stress. It is also shown that the influence of stress anisotropy on the small-strain shear modulus of sands is more pronounced for sands with irregular in shape grains and wider grain size distribution in comparison to uniform sands of relatively rounded and spherical grains. Based on the experimental results, a new G_{max} model is developed which incorporates the contribution of grain size characteristics and particle shape in the prediction of the small-strain shear modulus of sands subjected to stress anisotropy.

1. Introduction

Soil stiffness is a critical property for the seismic analysis of engineering geo-structures. Reliable evaluation of the stress-strain response of the soil, leading to a correct prediction of ground and structures deformations under static and dynamic loading, is directly dependent on the accurate assessment of the dynamic properties. Among dynamic properties of soil, shear modulus at small strains (below 10^{-3}%), typically denoted by G_{max}, is of particular interest in geotechnical engineering as well as the geophysical characterization of sediments.

According to the current body of literature, the small-strain shear modulus of dry and saturated sands is dependent on the void ratio (e) and the mean effective stress (p') resulting in the following general form for G_{max} ([3,4,6,7,13,16,20,21]):

$$G_{max(isotropic)} = A \times f(e) \times \left(\frac{P'}{p_a}\right)^n \quad (1)$$

in which $f(e)$ is the void ratio function, p_a is the reference atmospheric pressure for normalisation purposes and A and n are the model parameters which are functions of the coefficient of uniformity (C_u) and particle shape ([2,3,16,20]).

Most of the previous work on the small-strain shear modulus of granular soils has focused on the isotropic stress conditions. However, soils in earth structures, including natural soils under K_o condition or slopes, are invariably subjected to anisotropic stress conditions. Viggiani and Atkinson [22] and Jovicic and Coop [8] investigated the influence of deviatoric stress and anisotropic stress state on the small-strain shear modulus of reconstituted samples of Kaolin, and reported barely discernible effects. On the other hand, Rampello et al. [17] reported notably higher values of G_{max} for reconstituted clayey samples compressed anisotropically compared to those compressed isotropically at the same mean effective stress (p'). Using the results of tests performed in the true triaxial apparatus equipped with bender elements, it has also been shown that the small-strain shear modulus of sands is mainly influenced by the principal stresses in the direction of wave propagation and particle motion and is nearly independent of the out of plane stress component ([1,5,13,15,18,19,24,26,27,28]). Accordingly, the small-strain shear modulus model, Eq. (1), has been modified and extended for the general anisotropic stress state as ([1,5,15,18]):

$$G_{max(anisotropic)} = A_{ij}.\, f(e).\, OCR^k.\, \frac{\sigma_i'^{n_1}.\, \sigma_j'^{n_2}}{(p_a)^{n_1+n_2}} \quad (2)$$

where OCR is the overconsolidation ratio, A_{ij}, k, n_1 *and* n_2 are model parameters, and σ_i' and σ_j' are the principal effective stresses in the i and j directions, which correspond to the directions of

* Corresponding author.
E-mail address: n.khalili@unsw.edu.au (N. Khalili).

http://dx.doi.org/10.1016/j.soildyn.2016.06.004
0267-7261/

wave propagation and particle motion, respectively. This equation is however not consistent with the general G_{max} model for the isotropic condition as it does not reduce to Eq. (1) for the isotropic stress state. Moreover, following the critical state soil mechanics framework, only two out of the three state variables *e*, p' and *OCR* are required to identify the state of a given dry or saturated soil subjected to isotropic stresses; i.e. rendering the third state variable redundant ([16]). In addition, previous studies of the small-strain stiffness of anisotropically loaded granular soils have been limited to one or two specific types of sands; thus, the potential influence of different sand properties, including grain size characteristics and particle shape, have not been systematically investigated.

The main objective in this paper is to present results from a comprehensive program of laboratory testing on the small-strain shear modulus of sands subjected to stress anisotropy. Saturated specimens with a variety of particle shapes and grain size characteristics have been tested under different anisotropic stress states at constant mean effective stress. Particular attention is given to the contribution of principal stresses to the small-strain shear modulus of sands. It is shown that the increase in the small-strain shear modulus due to stress anisotropy is more pronounced in well-graded sands with angular particles, compared to poorly-graded material with rounded grains. Using the experimental results, a model is proposed for quantitative estimation of the effect of the stress anisotropy on the small-strain shear modulus of granular materials, incorporating the effects of both the grain size distribution and the shape of particles. Results from tests on several different sands subjected to constant stress ratios are used to demonstrate the verification and applicability of the model.

2. Development of a model for G_{max} of sands subjected to anisotropic stress state

In their previous work, the authors have developed a G_{max} model for sands under isotropic loading condition which, unlike other models in the literature, includes the effects of both gradation as well as particle shape ([16]). This model is used in this study as the basis for the development of a G_{max} model which includes the effect of anisotropic loading condition. To ensure consistency with the previous developments, the effective stress ratio is adopted for the incorporation of the effect of anisotropy through a power law relationship as follows:

$$G_{max(anisotropic)} = A \times f(e) \times \left(\frac{p'}{p_a}\right)^n (\eta + 1)^{\alpha(C_u, d_{50}, particle\ shape)} \quad (3)$$

where $\eta = q/p'$ is the effective stress ratio and α is a model parameter that is a priori function of the coefficient of uniformity (C_u), the mean grain size (d_{50}) and the particle shape as shown in Eq. (3).

Previous studies on the effect of anisotropy on G_{max} have shown that parameter α is closely related to n ([5,15,17,18]). Given that the parameter n is not a function of the mean grain size (d_{50}) for the granular soils with mean particle sizes less than 2 mm ([14,16,20,25]), parameter α is also assumed to be independent of the mean grain size (d_{50}). Furthermore, in the absence of evidence to the contrary, it is assumed that the effects of the coefficient of uniformity and particle shape on α can be decoupled, yielding the following reduced form for the small-strain shear modulus:

$$G_{max(anisotropic)} = A \times f(e) \times \left(\frac{p'}{p_a}\right)^n (\eta + 1)^{\alpha_1(C_u)\cdot\alpha_2(particle\ shape)} \quad (4)$$

To determine the dependency of the model parameters α_1 and α_2 to the grain size distribution properties and the shape of sand particles, respectively, a comprehensive series of tests on different sands having a variety of gradations and shapes are required.

3. Material used, experimental approach and testing program

3.1. Test materials

Nine different sands with a wide range of grain size distributions and particle shapes were tested, as listed in Table 1. Tests performed on sands BL1–BL5, with similar particle shapes, but different coefficients of uniformity (C_u), were used for the evaluation of the influence of gradation, while the results of the remaining experiments, including BL2, covering a wide range of particle shapes, were used to quantify the contribution of the particle shape to the small-strain shear modulus of saturated sands under anisotropic stress state. The particle size distribution curves of the test sands are shown in Fig. 1.

Particle shape descriptors, presented in Table 1, have been obtained in accordance with the particle shape characterization chart first introduced by [11] and then modified by [2]. The particle characterization chart identifies three shape descriptors to differentiate between regular and irregular particle shapes in a systematic manner. Shape descriptors, including roundness, sphericity and their arithmetic average referred to as regularity, can properly capture the shape of sand grains, as shown in Fig. 2 (a) for a typical particle. Roundness is quantified as the ratio of the average radius of the surface features to the radius of the largest sphere inscribed in the sand particle. Sphericity is an indication of the general shape of sand particles and is quantified as the ratio of the radius of the largest inscribed sphere in the particle to the smallest circumscribed sphere to the particle. Regularity is the

Table 1
Basic properties of test soils.

Sand name	*Sand type*	*Grain size distribution*			*Particle shape descriptors***					
		d_{50} (mm)	C_u*	C_c*	*R (MV)*	*S (MV)*	*ρ (MV)*	*R (SD)*	*S (SD)*	*ρ (SD)*
BL1	*Blue sand 1*	*1.66*	*1.41*	*0.94*	*0.24*	*0.51*	*0.38*	*0.12*	*0.18*	*0.15*
BL2	*Blue sand 2*	*0.69*	*2.00*	*1.01*	*0.24*	*0.51*	*0.38*	*0.12*	*0.18*	*0.15*
BL3	*Blue sand 3*	*1.94*	*2.80*	*0.97*	*0.24*	*0.51*	*0.38*	*0.12*	*0.18*	*0.15*
BL4	*Blue sand 4*	*1.88*	*4.11*	*1.22*	*0.24*	*0.51*	*0.38*	*0.12*	*0.18*	*0.15*
BL5	*Blue Sand 5*	*1.01*	*8.22*	*1.06*	*0.24*	*0.51*	*0.38*	*0.12*	*0.18*	*0.15*
50UB-50BL2	*50% Uniform bricky, 50% Blue sand 2*	*0.54*	*1.96*	*1.01*	*0.36*	*0.61*	*0.49*	*0.14*	*0.17*	*0.15*
B	*Bricky sand*	*0.47*	*2.19*	*1.18*	*0.48*	*0.71*	*0.60*	*0.16*	*0.15*	*0.16*
S	*Sydney sand*	*0.31*	*1.95*	*0.92*	*0.61*	*0.76*	*0.69*	*0.12*	*0.09*	*0.11*
W	*White (Blue circle) sand*	*0.24*	*1.69*	*0.90*	*0.71*	*0.76*	*0.74*	*0.14*	*0.11*	*0.13*

* $C_u = d_{60}/d_{10}$; $C_c = (d_{30})^2/(d_{10}.d_{60})$.
** R:Roundness, S:Sphericity, ρ:Regularity, MV:Mean Value, SD:Standard Deviation.

arithmetic average of roundness and sphericity. The regularity has been recently used by Payan et al. [16] in order to effectively capture the effect of particle shape on small-strain shear modulus of sands under isotropic loading conditions.

In order to quantify the shape descriptors for the tested materials, thirty randomly-selected particles from each sand were observed carefully through an optical microscope. The mean values (*MV*) for the roundness (*R*), the sphericity (*S*) and the regularity (ρ), as well as their corresponding standard deviations (*SD*) were recorded (summarized in Table 1) using the particle shape characterization chart shown in Fig. 2(b). The sand particles were placed under the microscope at their most stable state; accordingly, the effect of particle subjectivity due to the different particle positioning was not taken into account. It should be noted that the data presented in this study are only relevant to sands which are not subject to particle crushing, so that the shape of sand particles will not change during loading application. Consistent with Payan et al. [16], the regularity was selected as the shape descriptor for the development of the new G_{max} model to incorporate the combined effects of roundness and sphericity.

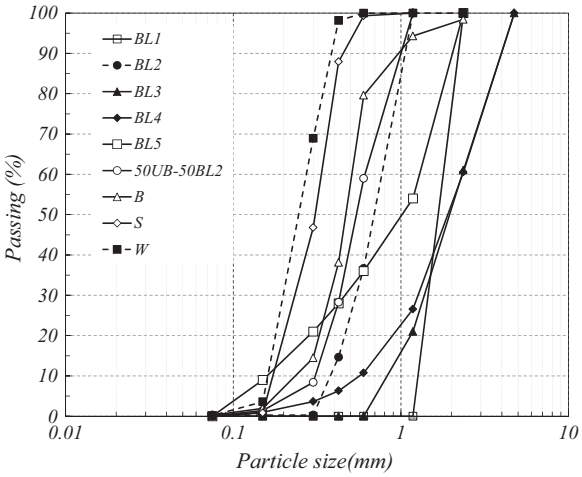

Fig. 1. Particle size distribution curves of test soils.

3.2. Sample preparation and experimental setup

In order to prepare soil samples, an adequate amount of material from each soil was first washed through the sieve No. 200 (0.075 mm opening size) to remove the fine-grained particles. Clean sands were then oven-dried at 105 °C for 24 h and subsequently left in the laboratory for at least 24 h to reach room temperature (air dry state in this study). The dried soils were then sieved to obtain the desired grain size distribution properties (C_u and d_{50}). The prepared sands were compacted in five layers into a

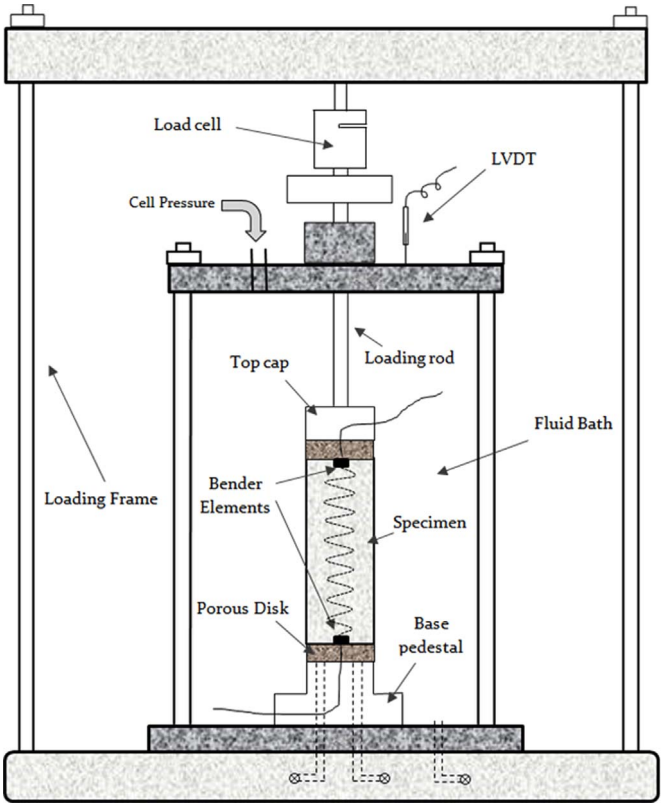

Fig. 3. Schematic diagram of the stress-path triaxial apparatus equipped with bender elements.

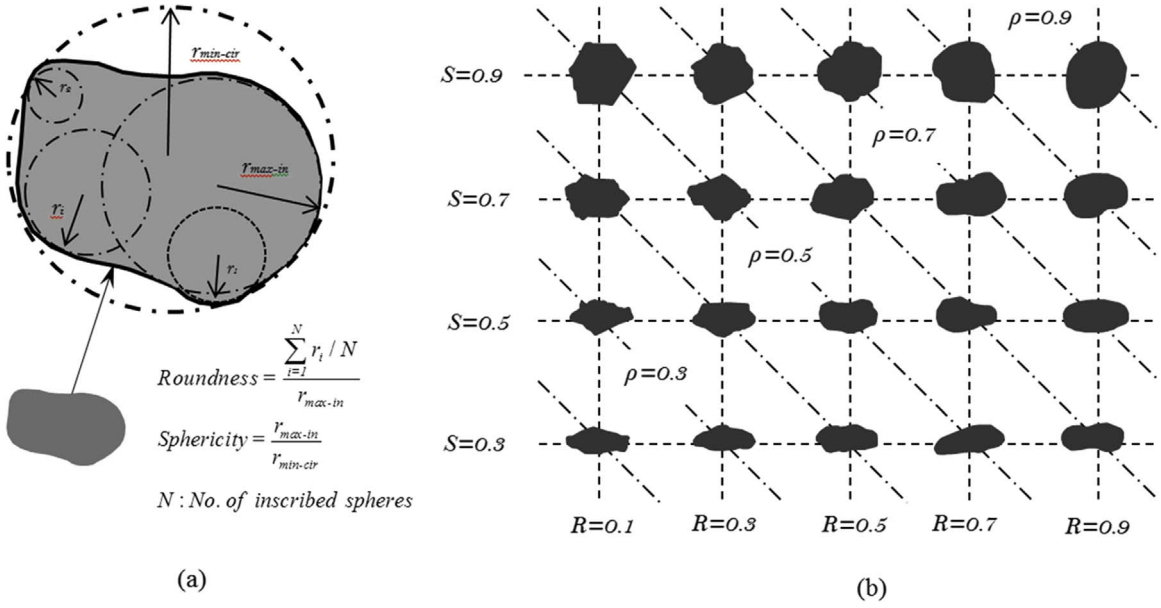

Fig. 2. Particle shape characterization chart (Modified from [11])

plastic mould directly on the base pedestal of the apparatus, using the wet tamping technique. The top of each layer was gently scarified prior to placing the next layer. The amount of energy applied to each soil layer was adjusted, so that the specimens could be prepared uniformly at a desired initial void ratio ([16]). The specimens, 10 cm in height and 5 cm in diameter, were saturated using the back pressure technique and checking the Skempton pore pressure parameter (B-value) at the end of each pressure step. A B-value of around 0.95 was considered as full-saturation.

A stress-path triaxial apparatus equipped with a pair of bender elements was used to perform the isotropic and anisotropic experiments on the sands. A schematic diagram of the device is shown in Fig. 3. The apparatus is capable of imposing complex stress paths, in the deviatoric versus the mean effective stress (q–p') plane. The bender elements utilised comprised piezoelectric ceramic bi-morphs, with the S-wave source insert attached to the top of the sample and the receiver insert attached to the bottom of the sample. A sinusoidal-type mode of excitation of the source insert was applied in the experiments with an amplitude of 14 V.

Table 2
Experimental program for model development.

Sample name	p' (kPa)	e_o	q (kPa)
BL1-1	*200*	*0.75*	*0-50-100-150-200*
BL1-2	*400*	*0.75*	*0-100-200-300-400*
BL1-3	*600*	*0.75*	*0-150-300-450-600*
BL2-1	*200*	*0.75*	*0-50-100-150-200*
BL2-2	*400*	*0.75*	*0-100-200-300-400*
BL2-3	*600*	*0.75*	*0-150-300-450-600*
BL2-4	*200*	*0.85*	*0-50-100-150-200*
BL2-5	*400*	*0.85*	*0-100-200-300-400*
BL2-6	*600*	*0.85*	*0-150-300-450-600*
BL3-1	*200*	*0.75*	*0-50-100-150-200*
BL3-2	*400*	*0.75*	*0-100-200-300-400*
BL3-3	*600*	*0.75*	*0-150-300-450-600*
BL4-1	*200*	*0.75*	*0-50-100-150-200*
BL4-2	*400*	*0.75*	*0-100-200-300-400*
BL4-3	*600*	*0.75*	*0-150-300-450-600*
BL5-1	*200*	*0.75*	*0-50-100-150-200*
BL5-2	*400*	*0.75*	*0-100-200-300-400*
BL5-3	*600*	*0.75*	*0-150-300-450-600*
50UB-50BL2-1	*200*	*0.75*	*0-50-100-150-200*
50UB-50BL2-2	*600*	*0.75*	*0-150-300-450-600*
B1	*200*	*0.75*	*0-50-100-150-200*
B2	*600*	*0.75*	*0-150-300-450-600*
S1	*200*	*0.75*	*0-50-100-150-200*
S2	*600*	*0.75*	*0-150-300-450-600*
W1	*200*	*0.75*	*0-50-100-150-200*
W2	*600*	*0.75*	*0-150-300-450-600*

3.3. Experimental program

In order to explore the influence of stress anisotropy on the small-strain shear modulus of sands, a comprehensive set of tests on saturated sands with a variety of gradations and particle shapes under anisotropic stress states was carried out. The experiments were conducted at constant mean effective stresses (p') of 200, 400 and 600 kPa and stress ratios (η) of 0, 0.25, 0.5, 0.75 and 1. The complete experimental program along with the initial void ratios of the specimens are summarized in Table 2. The stress paths followed during these experiments are graphically shown in Fig. 4. At each stress state, the shear wave velocity through the soil sample was measured using the bender elements embedded in the triaxial apparatus.

The variation of void ratio along the anisotropic loading paths under constant mean effective stress was recorded in all the tests based on the amount of water expelled from the specimen at each step. The effect of membrane penetration was taken into account using the procedure proposed by [10], which was found to be

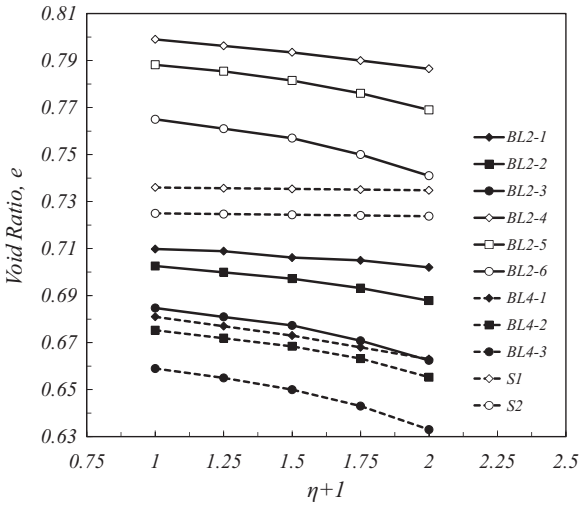

Fig. 5. Typical variation of void ratio during anisotropic loading at constant mean effective stress.

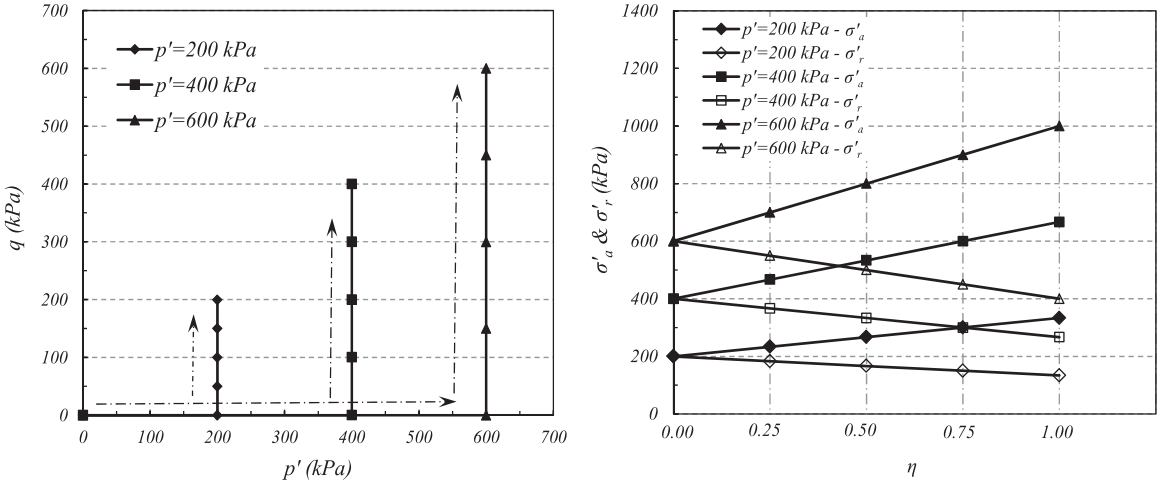

Fig. 4. Stress paths followed and stress points where bender element tests were performed.

negligible. Typical variations of the void ratio for different samples are shown in Fig. 5. As can be noted from this figure, although the decrease in void ratio of the specimens is not very significant along the anisotropic stress paths ($\Delta e_{max}=0.024$), the reduction in the void ratio is the greatest in the well graded angular sand subjected to the mean effective stresses of 600 kPa.

3.4. Interpretation of bender element test results

Shear wave velocity measurements in this study were performed using a pair of bender elements embedded to the top and bottom platens of the stress-path triaxial apparatus. The shear waves were propagated vertically through the samples resulting in a particle motion in the horizontal direction, capturing the small-strain shear modulus in the vertical-horizontal direction, typically denoted by G_{vh}. Small-strain shear moduli at other planes, i.e. G_{hh} and G_{hv} were not considered, as they require a different configuration of the bender element inserts.

Different approaches have been proposed in the literature for the selection of the first time arrival of shear waves in the interpretation of bender element test results ([9,12,23]). As an example of shear wave velocity interpretation in this study, typical results on the transmitted and received shear waves from the bender element tests on White sand under 200 kPa isotropic confining pressure at excitation frequencies of 2.5, 5, 7.5, 10, 12.5, 15 and 20 kHz are shown in Fig. 6. The arrows in this figure depict the selection of the first time arrivals of the shear waves in these tests. A brief discussion on the validity of this technique is given in Appendix A. A reference excitation frequency of 7.5 kHz was used in all the experiments to evaluate the first time arrivals of the

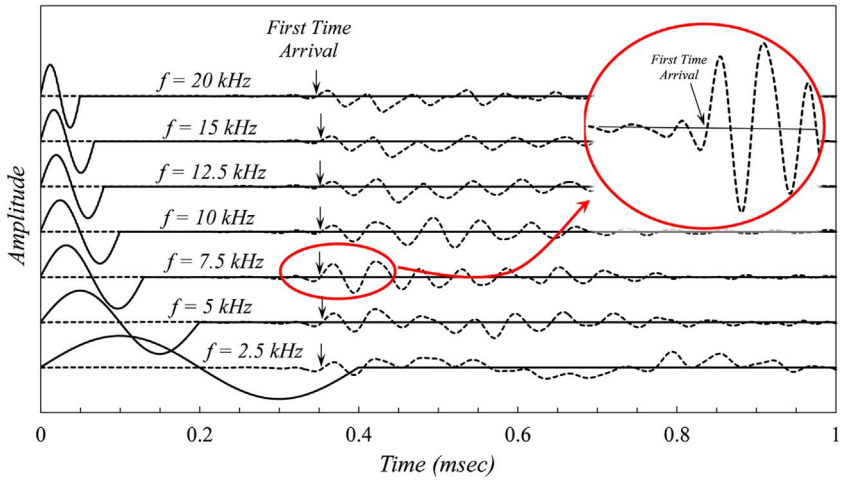

Fig. 6. Interpretation of bender element test results based on the first time arrival, White sand, $e_o=0.75$, $p'=200$ kPa, $q=0$ kPa, (Amplitude = 14 V, Vibration frequencies = 2.5, 5, 7.5, 10, 12.5, 15, 20 Hz).

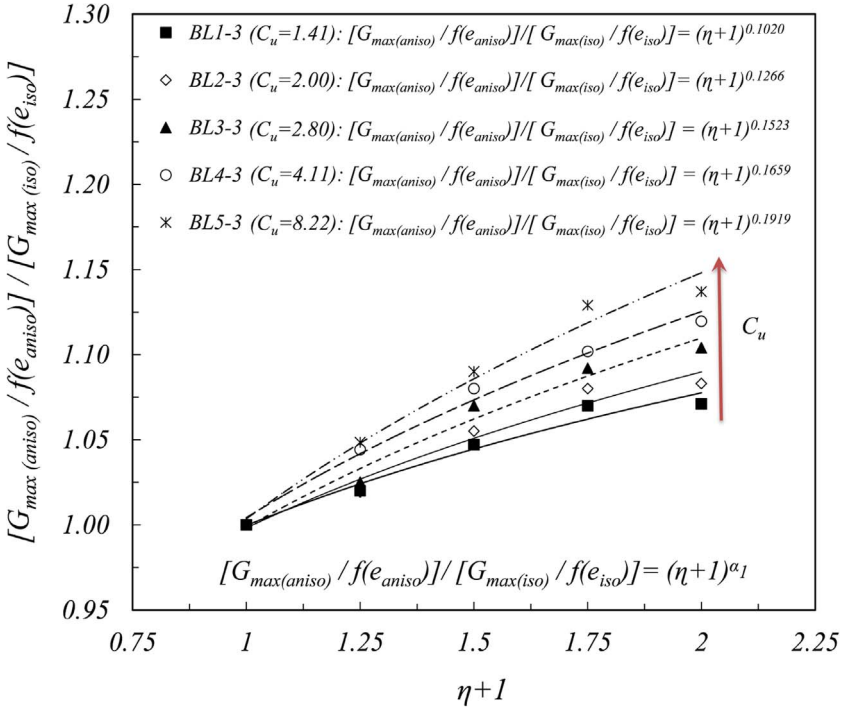

Fig. 7. Typical variation of normalised small-strain shear modulus with stress ratio for different gradations of Blue sand with the same particle shape subjected to 600 kPa mean effective stress.

shear waves. Using the tip-to-tip travel distance between the bender elements (L) and the travel time between the transmitted and received signals (t), the shear wave velocity (V_s) through the specimen, and consequently the small-strain shear modulus (G_{max}) of the soil were quantified as follow:

$$V_s = \frac{L}{t} \tag{5}$$

$$G_{max} = \rho V_s^2 \tag{6}$$

where ρ is the soil density.

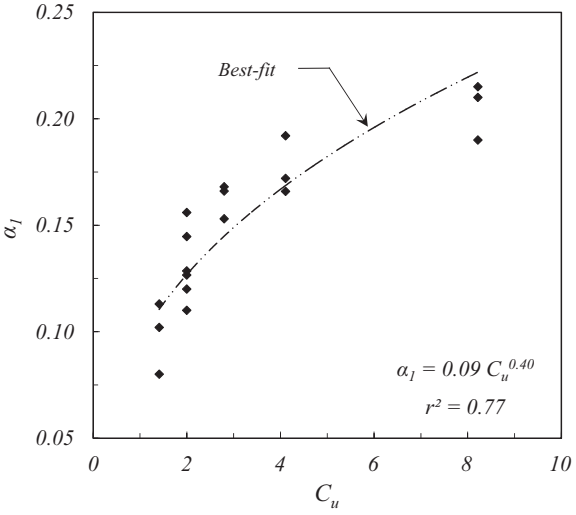

Fig. 8. Variation of α_1 with the coefficient of uniformity (C_u).

4. Results and discussion

4.1. The effect of coefficient of uniformity

In order to explore the influence of the coefficient of uniformity on the small-strain shear modulus of anisotropically loaded sands, the results of tests on different gradations of the Blue sand (BL1–BL5) with a specific particle shape were used.

To remove the effect of volume change and variations in void ratio on the small-strain shear moduli of the specimens subjected to anisotropic stress state, the values of G_{max} obtained from the test results at each deviatoric stress level were normalised with respect to the void ratio function previously proposed by Payan et al. [16]:

$$f(e) = e^{-1.29} \tag{7}$$

In this way, the effect of stress anisotropy could be captured through the ratio of the normalised small-strain shear modulus under isotropic and anisotropic stress states, i.e. $[G_{max(aniso)}/f(e_{aniso})]/[G_{max(iso)}/f(e_{iso})]$.

Fig. 7 shows a typical variations of normalised small-strain shear modulus, $[G_{max(aniso)}/f(e_{aniso})]/[G_{max(iso)}/f(e_{iso})]$, with respect to $(\eta+1)$ which are obtained for Blue sand specimens with different coefficients of uniformity subjected to the mean effective stress of 600 kPa. As can be observed from this figure, the small-strain shear moduli of sands under anisotropic loading are higher than those under isotropic stress state at the same mean effective stress. This accords with the previous observations of [1,5,15,18]. In addition, within the scatter of the data, the results for the anisotropically loaded samples show a clear power trend with respect to $\eta+1$.Using the best-fit curves to the data obtained for all Blue sand samples, the variation of α_1 (Eq. (4)) with the coefficient of uniformity (C_u) was obtained as (see Fig. 8):

$$\alpha_1 = 0.\ 09C_u^{0.40} \tag{8}$$

which implies an increasing influence of the effective stress ratio on the small-strain shear modulus with increasing coefficient of

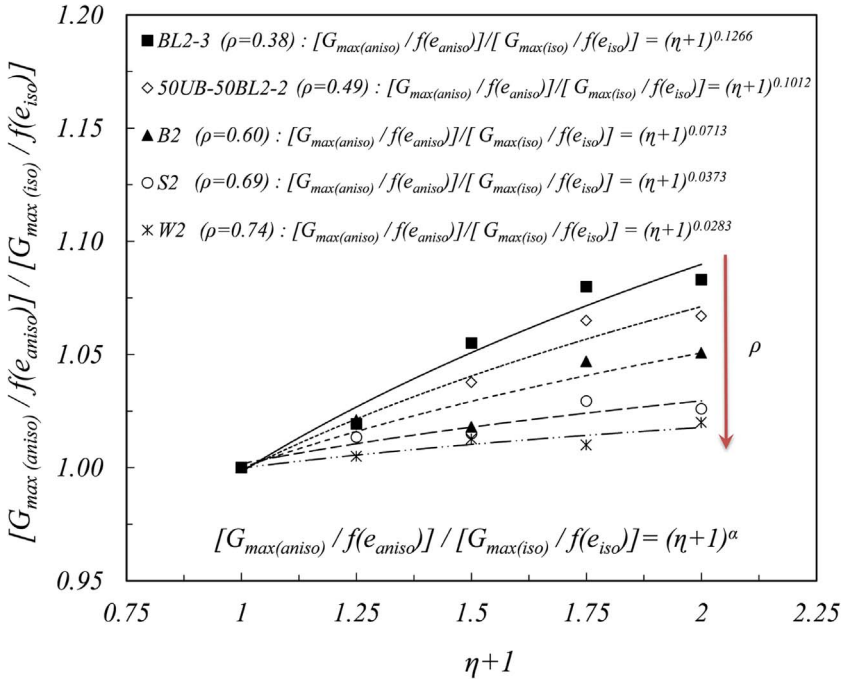

Fig. 9. Typical variation of normalised small-strain shear modulus with stress ratio for sands with different particle shapes in terms of regularity subjected to 600 kPa mean effective stress.

uniformity. This can be attributed partly to the greater structural stability of well-graded soils upon shearing due to the interlocking effect.

4.2. The effect of particle shape

To establish the impact of the shape of sand particles on the contribution of the stress anisotropy to G_{max}, the results of the experiments on BL2, 50UB-50BL2, B, S and W sands with particle shapes ranging from very angular and of low sphericity ($\rho=0.38$) to rounded and spherical ($\rho=0.74$), are used. Fig. 9 shows the typical variation of the normalised small-strain shear modulus, $[G_{max(aniso)}/f(e_{aniso})]/[G_{max(iso)}/f(e_{iso})]$, with respect to the measure of stress anisotropy ($\eta+1$) for sands with different regularities (ρ) subjected to 600 kPa mean effective stress. The figure shows that as ρ increases (the particles become more rounded), the effect of stress anisotropy on the small-strain shear modulus of soils becomes less pronounced. From the best-fit power trends to the data points using the least square error method, parameter α is obtained for each sample as shown in Fig. 9. Excluding the effect of the coefficient of uniformity through α_1 in Eq. (8), the effect of particle shape can be isolated by normalising α with α_1 as $\alpha_2=\alpha/\alpha_1$. The variation of α_2 against the three shape descriptors, i.e. roundness, sphericity and regularity, are plotted in Fig. 10 for all the samples tested. Fig. 10 shows that adopting the regularity as the shape descriptor can effectively capture the effects of roundness and sphericity through a single parameter without impacting on the goodness of fit. The following expression is obtained for α_2 with respect to ρ:

$$\alpha_2 = 0.19\rho^{-1.82} \tag{9}$$

which demonstrates the significant influence of particle shape on the small-strain shear modulus of sands subjected to anisotropic stress conditions. This phenomenon can be attributed to the rearrangement of sand particles upon shearing and development of the non-homogeneous contact normal forces among the particles. Particles of low regularity are more resistant against rotation during the application of anisotropic loads, rendering, perhaps, a more stable structure, stronger particle contacts and hence yielding a higher small-strain shear stiffness in their anisotropic stress state in comparison to the isotropic stress state.

5. A model for G_{max} of sands under anisotropic stress state

Using the best-fit equations derived in the previous sections, a general model can now be developed for capturing the effect of stress anisotropy in the prediction of the small-strain shear modulus of sands as follows:

$$G_{max(anisotropic)} = G_{max(isotropic)} \cdot (\eta+1)^{\alpha} \tag{10}$$

$$\alpha = 0.017\ C_u^{0.40}\rho^{-1.82} \tag{11}$$

This model is general in the sense that any $G_{\max(isotropic)}$ model can be adopted in Eq. (10). In this study, the $G_{\max(isotropic)}$ model proposed by [16] is used for this purpose leading to the following explicit $G_{\max(anisotropic)}$ model:

$$G_{max(anisotropic)} = 84C_u^{-0.14}\rho^{0.68}e^{-1.29}\left(\frac{p'}{p_a}\right)^{(C_u^{0.12})(-0.23\rho+0.59)} (\eta+1)^{(0.017C_u^{0.40}\rho^{-1.82})} \tag{12}$$

A close examination of this expression reveals that the contribution of the two principal stresses (in the direction of the wave propagation and the direction of particle motion) in the $G_{\max(anisotropic)}$ are generally different. In this regard, the contribution of the principal stress acting in the direction of wave propagation is more than that in the direction of particle motion. Furthermore, the difference between the contributions of the two principal stresses is more considerable for well-graded sands having irregular in shape particles compared to the poorly-graded soils having relatively rounded and spherical particles, as for sands with sub-rounded or rounded particles, the principal stresses have almost the same contributions on the small-strain shear modulus.

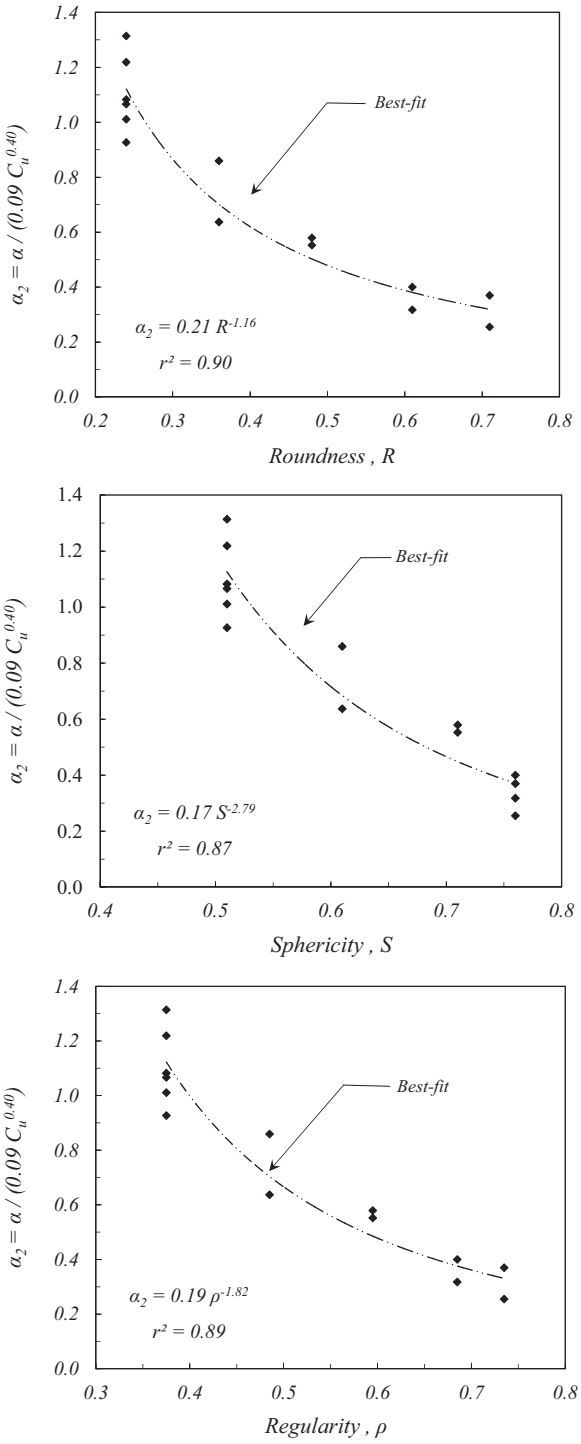

Fig. 10. Variation of parameter α_2 with Roundness (R), Sphericity (S) and Regularity (ρ).

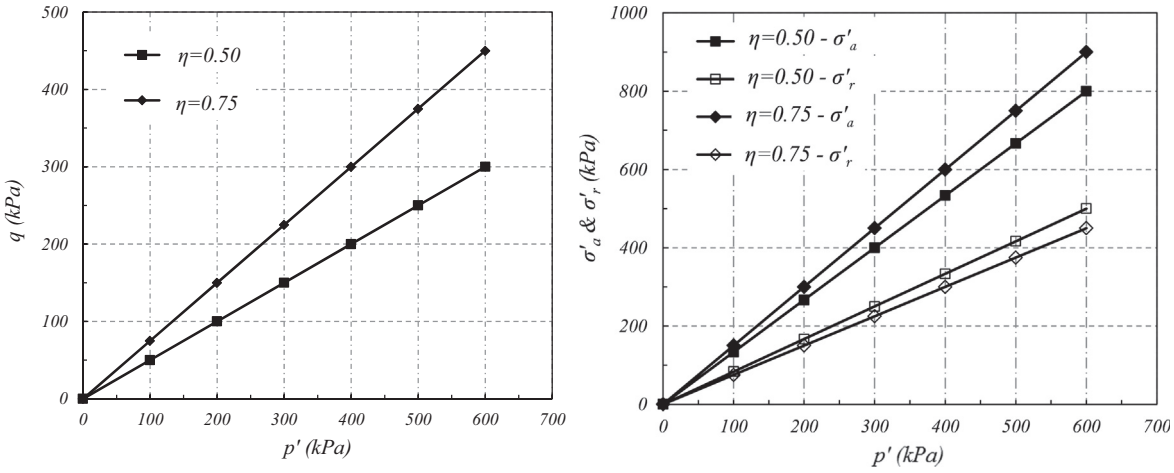

Fig. 11. Verification tests: stress paths followed and stress points where bender element tests were performed.

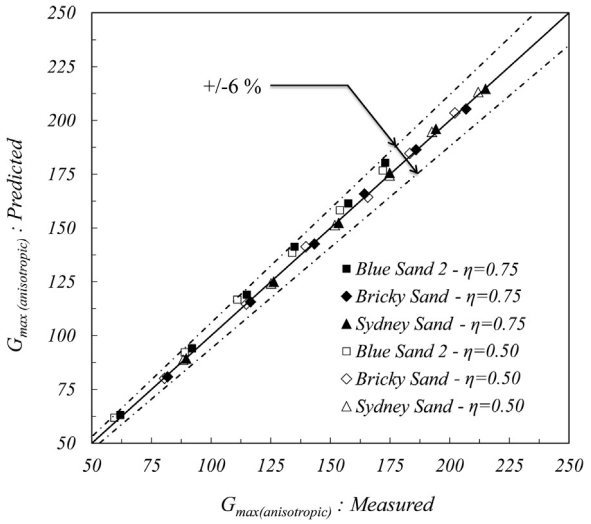

Fig. 12. Measured versus predicted values of $G_{max(anisotropic)}$ at constant stress ratios of 0.50 and 0.75 for Blue 2, Bricky and Sydney sands.

6. Verification of the proposed model

In order to verify the validity of the proposed model for the prediction of the small-strain shear modulus of sands subjected to an anisotropic stress state (Eq. (12)), six additional sets of tests have been performed on three different saturated sands, i.e. Blue sand 2, Bricky sand and Sydney sand. The stress path of constant stress ratio was selected for the verification tests as opposed to the constant mean effective stress used in the development of the model. Specimens were prepared at the same initial target void ratio of 0.75 using the wet tamping method explained before and were subjected to constant stress ratios of 0.50 and 0.75. The variations of the axial and radial stresses and the stress paths followed during these tests are shown in Fig. 11. The bender element tests were performed at a sequence of mean effective stresses of 100, 200, 300, 400, 500 and 600 kPa, in order to measure the shear wave velocity and the small-strain shear modulus of the test sands.

The $G_{max\ (anisotropic)}$ values for the verification tests are also predicted directly using the newly developed model in this study (Eq. (12)) and compared to the experimentally obtained values, as shown in Fig. 12. As can be seen from this figure, the predicted $G_{max\ (anisotropic)}$ values are in excellent agreement with the measured ones (with the maximum error of less than 6%), confirming the applicability of the proposed model for the prediction of the small-strain shear modulus of sands under anisotropic loading condition.

7. Concluding remarks

The small-strain shear modulus of sands subjected to anisotropic state of stress was investigated through a comprehensive set of experiments on saturated samples using a stress-path triaxial apparatus equipped with a pair of bender elements. The influence of different sand properties, including the grain size characteristics and the particle shape, and anisotropic stress state on the small-strain shear modulus of sands was studied. Considering the effects of volume and void ratio changes during anisotropic loading, it has been generally shown that the stress anisotropy has a considerable influence on the small-strain shear modulus of sands, resulting in higher values of G_{max} for soils under anisotropic stress state compared to those subjected to isotropic confining pressure at a given mean effective stress. It has also been observed that the increase in the small-strain shear modulus of sands due to stress anisotropy becomes more pronounced as the angularity of the particles and the coefficient of uniformity increase. This has been attributed, partly, to the higher structural stability and non-homogeneous distribution of contact normal forces among the particles of test sands due to shearing. Based on the experimental results, a new model has been developed for the prediction of the small-strain shear modulus of sands subjected to anisotropic loading conditions. The newly proposed model has been verified using the results of six sets of bender element tests on three different sands performed along constant stress ratio paths. Excellent agreement is obtained between measured and predicted values.

Appendix A

To validate the method used in this study for the estimation of the first-time arrival of shear waves, the authors have conducted a comprehensive program of laboratory testing on different sands, with different void ratios, under various isotropic stresses, using both bender elements and resonant column tests. It is found that the proposed technique yields small-strain shear moduli that are in best agreement with the results obtained from the resonant column tests in torsional mode of vibration. A typical of the comparative results for Sydney sand with initial void ratios of 0.66,

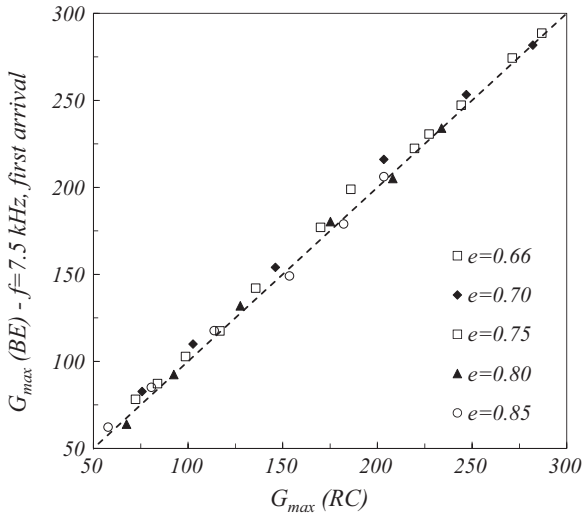

Fig. A1. Comparison between bender element and resonant column test results for Sydney sand.

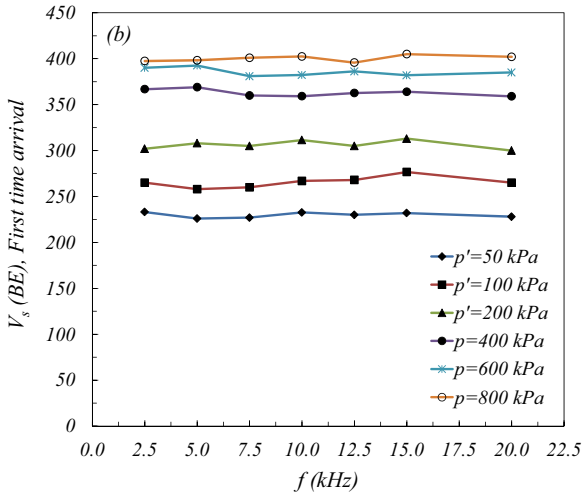

Fig. A2. Effect of input frequency on the shear wave velocity measurements for Sydney sand.

0.70, 0.75, 0.80 and 0.85 subjected to isotropic stress states of 50, 100, 200, 400, 600 and 800 kPa is shown in Fig. A1. Note that the results from the bender element tests in this figure corresponded to a frequency of 7.5 kHz. The figure clearly shows that the small-strain shear moduli obtained from the bender element tests using the above interpretation approach are in excellent agreement with those obtained using the resonant column tests, confirming the correct interpretation of the first time arrivals of the shear waves.

In addition, Fig. A2 shows the insensitivity of the shear wave velocity measurements to the excitation frequency for Sydney sand at an initial void ratio of 0.75.

References

[1] Bellotti R, Jamiolkowski M, Lo Presti DCF, O'Neill DA. Anisotropy of small strain stiffness in Ticino sand. Geotechnique 1996;46(1):115–31.
[2] Cho GC, Dodds J, Santamarina JC. Particle shape effects on packing density, stiffness, and strength: natural and crushed sands. J Geotech Geoenviron Eng 2006;132(5):591–602.
[3] Edil TB, Luh G-F. Dynamic modulus and damping relationships for sands. Soil Dyn Earthq Eng 1978;1:394–409.
[4] Hardin BO, Black WL. Sand stiffness under various triaxial stresses. J Soil Mech Found Div 1968;94(SM2):353–69.
[5] Hardin BO, Blandford GE. Elasticity of particulate materials. J Geotech Eng 1989;115(6):788–805.
[6] Hardin BO, Richart Jr. FE. Elastic wave velocities in granular soils. J Soil Mech Found Div 1963;89(1):33–65.
[7] Iwasaki T, Tatsuoka F. Effects of grain size and grading on dynamic shear moduli of sands. Soils Found 1977;17(3):19–35.
[8] Jovičić V, Coop MR. The measurement of stiffness anisotropy in clays with bender element tests in the triaxial apparatus. Geotech Test J 1998;21(1):3–10.
[9] Jovičić V, Coop MR, Simic M. Objective criteria for determining G_{max} from bender element tests. Geotechnique 1996;46(2):357–62.
[10] Kramer SL, Sivaneswaran N, Davis RO. Analysis of membrane penetration in triaxial test. J Eng Mech 1990;116(4):773–89.
[11] Krumbein WC, Sloss LL. Stratigraphy and sedimentation. 2nd ed.. San Francisco: Freeman and Company; 1963.
[12] Lee JS, Santamarina JC. Bender elements: performance and signal interpretation. J Geotech Geoenviron Eng 2005;131(9):1063–70.
[13] Lo Presti D, O'Neill DA. Laboratory investigation of small strain modulus anisotropy in sand. In: calibration chamber testing: proc., first int. symp. on calibration chamber testing/ISOCCT1. Elsevier, New York; 1991, p. 213–24.
[14] Menq FY. Dynamic properties of sandy and gravelly soils [Ph.D. Dissertation]. Austin, TX: University Of Texas at Austin; 2003.
[15] Ni SH. Dynamic properties of sand under true triaxial stress states from resonant column and torsion shear tests [Ph.D. thesis]. 1987, The University of Texas in Austin.
[16] Payan M, Khoshghalb A, Senetakis K, Khalili N. Effect of particle shape and validity of G_{max} models for sand: a critical review and a new expression. 2016, Computers and Geotechnics. vol. 72, p. 28–41.
[17] Rampello S, Viggiani GMB, Amorosi A. Small-strain stiffness of reconstituted clay compressed along constant triaxial effective stress ratio paths. Geotechnique 1997;47(3):475–89.
[18] Roesler SK. Anisotropic shear modulus due to stress anisotropy. J Geotech Eng Div 1979;105(GT7):871–80.
[19] Santamarina JC, Cascante G. Stress anisotropy and wave propagation: a micromechanical view. Can Geotech J 1996;33:770–82.
[20] Senetakis K, Anastasiadis A, Pitilakis K. Small strain shear modulus and damping ratio of quartz and volcanic sands. Geotech Test J 2012;35(6):1–17.
[21] Stokoe KH II, Hwang SK, Lee JNK, Andrus RD. Effects of various parameters on the stiffness and damping of soils at small to medium strains. In: prefailure deformation of geomaterials: proc., int. symp. on pre-failure deformation characteristics of geomaterials. Balkema, Rotterdam; 1995, p. 785–816.
[22] Viggiani G, Atkinson JH. Stiffness of fine-grained soil at very small strains. Geotechnique 1995;45(2):249–65.
[23] Viggiani G, Atkinson JH. Interpretation of bender element tests. Geotechnique 1995;45(1):149–54.
[24] Wang YH, Mok CMB. Mechanisms of small-strain shear modulus anisotropy in soils. J Geotech Geoenviron Eng 2008;134(10):1516–30.
[25] Wichtmann T, Triantafyllidis T. Influence of the grain-size distribution curve of quartz sand on the small strain shear modulus G_{max}. J Geotech Geoenviron Eng 2009;135(10):1404–18.
[26] Yamashita S, Hori T, Suzuki T. Effects of initial and induced anisotropy on initial stiffness of sand by triaxial and bender elements tests. In: Yamamuro AJ, Koseki J, editors. Geomechanics: testing, modeling, and simulation (GSP 143). Reston, Va.: ASCE; 2005. p. 350–69.
[27] Yu P, Richart FE. Stress ratio effects on shear modulus of dry sands. J Geotech Eng 1984;110(3):331–45.
[28] Zeng X, Ni B. Stress-induced anisotropic G_{max} of sands and its measurement. J Geotech Geoenviron Eng 1999;125(9):741–9.